Influence of the amphiphilicity profile of copolymers on the formation of liquid crystalline mesophases in microemulsions

Helge F. M. Klemmer[1]

Department of Chemistry, University of Cologne, Luxemburger Straße 116, 50939 Cologne, Germany.

J. Allgaier[2]

Jülich Centre for Neutron Science JCNS and Institute for Complex Systems ICS, Forschungszentrum Jülich GmbH, 52425 Jülich, Germany

Henrich Frielinghaus[3], Olaf Holderer[3*]

Jülich Centre for Neutron Science JCNS at MLZ, Forschungszentrum Jülich GmbH, Lichtenbergstraße 1, 85747 Garching, Germany; Fax: +49 89 289 10799; Tel: +49 89 289 10707; E-mail: o.holderer@fz-juelich.de

Michael Ohl[4]

Jülich Centre for Neutron Science JCNS at SNS, Forschungszentrum Jülich GmbH, POB 2008, 1 Bethel Valley Rd., Oak Ridge, TN 37831-6473, USA

*Corresponding author

Abstract

In bicontinuous microemulsions, the increase of the solubilisation capacity of a surfactant, e.g. by the addition of amphiphilic block copolymers ("boosting effect") is normally accompanied by the formation of liquid crystalline mesophases. We studied a new class of amphiphilic polymers as "boosters", so called gradient polymers, with a gradual change from the hydrophilic to the hydrophobic part. Phase diagram measurements and static and quasielastic neutron scattering experiments reveal that the polymers cause a stiffening of the amphiphilic film while simultaneously the saddle splay modulus decreases such that the formation of liquid crystalline mesophases, normally present with diblock polymers as "boosters", is suppressed, while bicontinuous structures are geometrically favoured. In addition these findings are supported by theoretical calculations following the works of *Lipowsky*. Hence gradient amphiphilic polymers not only increase the efficiency of surfactants but simultaneously suppress the formation of liquid crystalline phases thereby greatly increasing their application potential.

1. Introduction

Despite their multitude of beneficial properties, like ultra-low interfacial tension [1], tunable nanostructure [2, 3] and thermodynamic stability [4-7] microemulsions lack general application. This is mainly due to the comparably high amounts of surfactant required to formulate a balanced microemulsion. In 1999 *Strey* and coworkers utilized amphiphilic diblock copolymers as so-called efficiency boosters to dramatically reduce the amount of amphiphiles to prepare a microemulsion [8]. The diblock copolymers act as a much larger version of a surfactant molecule, with the hydrophilic block sitting on the water side of the surfactant membrane like a mushroom, the hydrophobic part on the oil side of the membrane. While they observed the suppression of lamellar phases, which usually accompany highly efficient microemulsions [9], for very low polymer content, increasing the polymer content leads to even more pronounced lamellar and other mesophases, that completely cover the desired isotropic microemulsion phase [10-12]. In the following years, more research regarding amphiphilic polymers and their effect on microemulsions was conducted and lead among other things to an explanation for the occurring effects [13-15]. Simultaneously different types of polymers like sticker polymers [16, 17] , bola polymers [18], gradual polymers [19, 20] or star-shaped polymers [21, 22] were designed. While for some of these polymers a similar boosting effect was observable, also "anti-boosting" could be shown, but not fully explained [23-25] . Lately, a new type of polymer emerged, that does not include the common diblock or multiblock structure. These so called tapered or gradient polymers feature a gradual structure, wherein the nature of polarity changes gradually from hydrophilic to hydrophobic along the polymer chain with additional hydrophilic and hydrophobic terminal domains (see [26-28] and references therein). Whereas gradient copolymers directly go gradually from one type to the other, tapered polymers contain pure blocks of one or the other type at both ends similarly to a diblock copolymer. In 2013 *Allgaier et al*. resolved the composition profile for tapered and gradient copolymers of ethyleneoxide and 1,2-butyleneoxide [29] and the question arose regarding their potential as efficiency boosters. In this paper we report on the efficiency boosting of gradient copolymers and display a structure - mode of action correlation regarding the effect of the gradient copolymers by starting with diblock copolymers and systematically changing their structural nature via triblocks containing a moderately polar middle block until a gradient copolymers is reached. The gradient polymer has a pure PBO side on one end (as for a tapered polymer), and a EO rich opposite side and is in this way partly a pure tapered, partly strictly speaking a gradient polymer. In the following we stick to the nomenclature of a gradient polymer. First, a short introduction into the theory of membranes is given.

2. Theory

In literature, the theory for single-sided anchored polymers [30-33] (and later for free polymers [34]) has been developed. The anchoring point of amphiphilic diblock copolymers seems to be defined exactly [14, 15, 35], and anchoring conditions for single-sided sticker polymers have been examined [16, 17]. For the anchored polymers, it was assumed that only the conformational entropy of the polymer acts as an additional term on the bending rigidity. This means that the anchoring is not questioned, and no gradual energetic terms do appear for the whole problem. For ideally gradient polymers, the anchoring is accompanied with a gradual energy of $\varepsilon(N_1-N/2)^2$ that describes the dependence on the block length N_1 in the aqueous domain for a symmetric polymer with the degree of polymerization N (N-N_1 is the block length in the oil domain). The energetic parameter ε in relative units to the thermal energy k_BT is high ($\varepsilon \gg 1$) for strong anchoring and low for loose anchoring. This means that for a diblock polymer, the anchoring point (the part of the polymer which is inside the surfactant membrane) is the position where the amphiphilic and hydrophilic parts are connected, and the parts which are on the oil side and water side are the complete hydrophobic and hydrophilic blocks respectively. In the case of the gradient polymer, the loosely anchored gradual transition region (instead of the abrupt transition) can slide more to the oil- or water-side respectively.

In *Lipowsky*'s theory [31-33] for anchored polymers the partition function is purely entropic and reflects the polymer conformations. As analytic terms become complicated, the expansions of the partition function in the limit of weakly curved surfactant membranes were examined. From these considerations the purely entropic free energy was calculated and then compared to the curvature dependence of a free energy of a membrane, from which the polymer influence on the bending rigidity and saddle splay modulus was derived.

In parallel to these considerations we extend the partition function to multiple realizations of the anchoring point and extend the purely entropic partition functions $Z(N_1)$ and $Z(N\text{-}N_1)$ of single-sided blocks by the energetic term described above. The partition function of an ideally gradient polymer anchored in a membrane then reads:

$$Z_{\text{tot}} = \int_0^N dN_1 \exp\left(-\varepsilon\left(N_1 - \left(\frac{N}{2}\right)\right)^2\right)\left(Z(N_1)\cdot Z(N-N_1)\right) \qquad (1)$$

The considerations after that follow the ideas of *Lipowsky*, the terms of which are derived to asymptotically weak curvatures for spherical and cylindrical membranes, and then related to the bending rigidity κ and saddle splay modulus $\bar{\kappa}$. More details are given in the

supplementary material. The characteristic coefficients Ξ and $\bar{\bar{\Xi}}$ for the two elastic moduli κ and $\bar{\kappa}$ are free from trivial dependencies of the polymer concentration (or grafting density σ) and the polymer size in terms of the typical end-to-end distance of the free polymer ($R_{ee,o}$ and $R_{ee,w}$, in the oil and water domain):

$$\frac{\kappa}{k_B T} = \frac{\kappa_0}{k_B T} + \Xi\sigma(R_{ee,o}^2 + R_{ee,w}^2) \tag{2}$$

$$\frac{\bar{\kappa}}{k_B T} = \frac{\overline{\kappa_0}}{k_B T} - \bar{\bar{\Xi}}\sigma(R_{ee,o}^2 + R_{ee,w}^2) \tag{3}$$

Note that the polymer size in this dependence does not depend on the anchoring point, because for each block $R_{ee,i}^2 \sim N_i$., and an asymmetrically locked polymer would have the same change in the elastic moduli as the symmetric diblock copolymer. The relative dependence of the two characteristic coefficients Ξ and $\bar{\bar{\Xi}}$ as a function of the normalized anchoring strength εN^2 is discussed in theory and compared with the experimental findings of this manuscript in context to Figure 2.1. For weak anchoring the parameter εN^2 is around 1 to 10, and for well-defined anchoring it is above 1000 up to virtually infinity. The relative dependence of the coefficients stays nearly unchanged from the ideal diblock copolymer for anchoring parameters above 30, and can reach 30% to 40% diminished values in the limit of tapering with loosely defined anchoring. This arises from the additional degree of freedom that allows the polymer to give way to the membrane curvature. Experimentally, the general dependence is confirmed for the saddle splay modulus $\bar{\kappa}$ and its coefficient $\bar{\bar{\Xi}}$. Using small angle neutron scattering (SANS), the relative change of the coefficient Ξ for the gradient polymer is much stronger than predicted, while using neutron spin echo (NSE) spectroscopy there seems to be no considerable dependence of Ξ. Thus, the coefficient of the bending rigidity seems to depend on the experimental method, and is in the focus of this study.

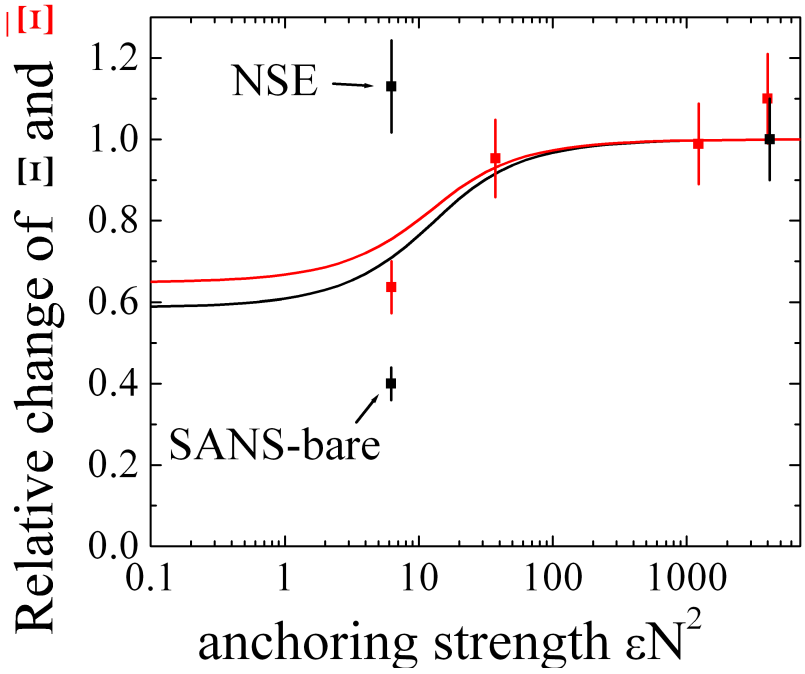

Figure 2.1: The relative changes of the polymer effect on the bending rigidity and saddle splay modulus, expressed by the coefficients Ξ and $\bar{\Xi}$, as a function of the anchoring strength. The theory is depicted as continuous lines, while data points correspond to different polymers: gradient polymer, triblock copolymer with longer / shorter mid-block, and diblock copolymer (from left to right). For the gradient polymer, the change of Ξ depends on the experimental method (NSE and SANS).

3. Experimental

3.1 Materials

Water was double-distilled using a quartz column and *n*-decane was purchased with a purity > 99.50% from Fulka AG, Buchs, Switzerland (batch-no. 20396APV). The surfactant tetraethyleneglycol-mono-*n*-decylether ($C_{10}E_4$) was purchased from Bachem, Bubendorf, Switzerland at a purity > 97% with a critical temperature $T_C = 33.48$ °C for the binary aqueous mixture (batch-no. 1027622). The experimental technical grade amphiphilic poly(ethylene/butylene)-b-polyethyleneoxide diblock copolymer Tego EBE 55x (1) (PEB4.8 - PEO4.8, with 4.8 kg/mol per block) with the batch-no. 95E001 was a gift from the Th. Goldschmidt AG, Essen, Germany. The copolymer itself was supplied at 45% purity with the remainder being xylene residues originating from its synthesis. Before use, the copolymer was dried at elevated temperatures ($T = 40$ °C) and reduced pressure ($p = 50$ mbar) for two weeks to constant mass.

The diblock PBO5 - PEO5 was synthesized as explained in reference [36] using ethylene oxide (EO) and 1,2-butylene oxide (BO) as monomers. The triblocks PBO5 - PPO0.5 - PEO5 and PBO4 - PPO3 - PEO4 were synthesized in a modified way as PBO-PPO diblock intermediates always contained some poly propylene oxide (PPO) homopolymer. The synthesis of PBO5 - PPO0.5 - PEO5 and PBO4-PPO3-PEO4 is described in the supplementary materials. For the gradient copolymer P(BO/EO)22 both monomers were polymerized simultaneously. In anionic ring opening polymerization EO polymerizes visibly faster than BO. As a consequence at the beginning of the polymerization mainly EO is incorporated into the growing polymer chains whereas the final sections only consist of BO units. In between the monomer composition gradually changes. Figure 3.2 shows the calculated compositional profile in terms of the fraction of EO units using the rate constants and the kinetic model described in reference [29]. The polymerization of P(BO/EO)22 was carried out using the low temperature approach in combination with 18-crown-6. Because of the insolubility of the PEO rich initial chain sections in cold toluene the polymerization temperature was raised to 10 °C, compared to -10 °C to -20 °C normally used for the homopolymerization of BO. Nevertheless, the molecular weight distribution of the product was narrow (Table 3.1).

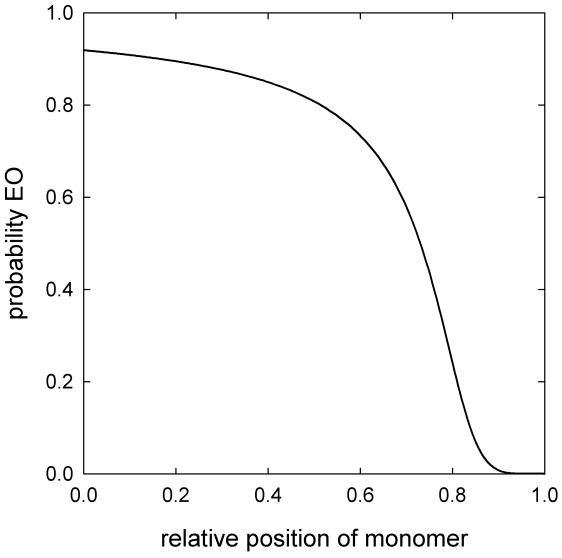

Figure 3.2: Calculated compositional profile of the gradient copolymer P(BO/EO)22.

The molecular weights, molecular weight distributions and compositions of the polymers are summarized in table 3.1. The numbers in the sample name (e.g. PBO5) indicate the molecular weight of this block in 10^3 g/mol.

Table 3.1: Composition of the amphiphilic polymers used within this paper and the supplementary material. All polymers have approximately the same size as their molar mass is almost equal. For more details regarding the synthesis see text.

Polymer	Block molecular weight ratio	M_n [g/mol]	M_w/M_n
PEB4.8 - PEO4.8	1.00 : 0 : 1.00	9600	-
PBO5 - PEO5	1.00 : 0 : 1.01	11400	1.02
PBO5 - PPO0.5 - PEO5	1.00 : 0.12 : 1.02	12100	1.02
PBO4 - PPO3 - PEO4	1.00 : 0.74 : 0.96	10900	1.01
P(BO/EO)22 (gradient)	1.00:1.17*	21800	1.01

*overall BO/EO molecular weight ratio

Based on the phase behavior measurements given in the results and the supplementary material all polymers are equal to the nonionic surfactant $C_{10}E_4$ with regard to polarity and amphiphilicity. This can be deduced as upon polymer addition no shift in temperature and phase sequence can be observed. All other chemicals were used as purchased and without further purification.

3.2 Microemulsion Sample Preparation

In general the microemulsion samples with a total mass of m = 0.5 g were prepared such, that first the surfactant and the polymer were given into a gas tight sample tube, whereby the composition is controlled by weight with an accuracy of $\Delta m = \pm 0.0005$ g. Then, first the non-polar followed by the polar components were added. Regarding the $T(\gamma)$-phase diagrams the overall composition of the samples is defined by the volume ratio of the polar component A and the non-polar component B

$$\phi = \frac{V_B}{V_A + V_B} \tag{4}$$

the overall mass fraction of surfactant C and polymer D

$$\gamma = \frac{m_C + m_D}{m_A + m_B + m_C + m_D} \tag{5}$$

the mass fraction of polymer D in the surfactant/polymer mixture

$$\delta = \frac{m_D}{m_C + m_D} \tag{6}$$

The mass fraction δ of the polymer is related to the mass of the membrane in the microemulsion, the typical values of 10-20% mean therefore at 10% surfactant contents that the total polymer contents in the sample is of the order of 1-2%.

After placing the sample tube in a thermostated water bath, the sample is stirred with a magnetic stirring bar until macroscopically homogeneous at approximately the phase inversion temperature of the polymer-free system $T \approx 30$ °C. This process usually takes 5 minutes, but to ensure equilibration the sample was stirred for 1 h. To determine the phase upon reaching thermal equilibrium, the stirrer is stopped and the number and nature of coexisting phases is checked by visual inspection of scattered and transmitted light. Anisotropic (L_α) and shear-anisotropic phases (V_1 and V_2) are identified using crossed polarizers. Phase boundaries are generally determined after waiting for complete phase separation (usually 1 h) and by continuously readjusting the temperature. The boundaries given here have an accuracy of $\Delta T = 0.05$ °C. Generally speaking phase behavior was determined as published by *Kahlweit* and *Strey*. For more details we refer to Ref [5]. A simple phase diagram is given in figure 3.3 including pictures to explain the optically visible features of phase states.

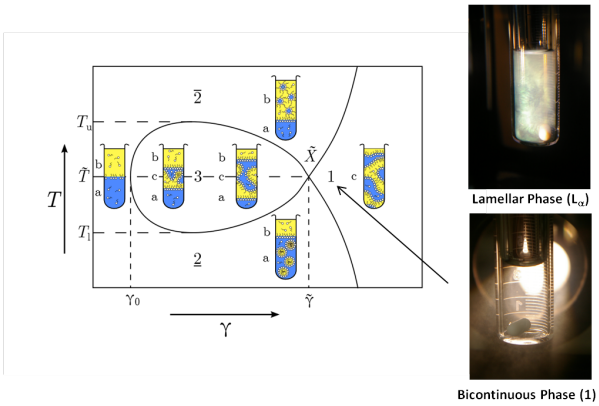

Figure 3.3: Exemplary phase diagram with a nonionic phase sequence redrawn and modified based on [5]. The right hand side pictures exemplarily display a lamellar L_α phase viewed through crossed polarizers (top) and the isotropic bicontinuous one phase region 1 (bottom).

3.2 Neutron Scattering Experiments

All small angle neutron scattering (SANS) experiments were performed at the KWS-1 instrument operated by JCNS at the Heinz Maier-Leibnitz Zentrum (MLZ), Garching, Germany, while the neutron spin echo (NSE) measurements were conducted at the SNS-NSE instrument at the spallation neutron source at the Oak Ridge National Laboratory (ORNL).

While the SANS samples were all prepared in bulk contrast by replacing water with equal volume of heavy water, the NSE experiments were done in film contrast matching the scattering length densities of the polar and the nonpolar phase using deuterated oil. The respective samples were all prepared at amphiphile concentrations corresponding to the concentration at the optimal point of the polymer-free microemulsion and the phase inversion temperature of each sample. More details regarding each individual sample are given in the results section. Temperature stability of the samples was ensured by using a furnace with $\Delta T = \pm 0.1$ K. Details regarding data analysis are given in the results section. All data were reduced using the latest version of QtiKWS as supplied by JCNS.

4. Results

In the following the influence of the synthesized diblock copolymer and the gradient polymer on the phase behavior of the microemulsion system H_2O/NaCl - *n*-decane - $C_{10}E_4$/polymer will be given in detail, while the synthesis of the polymers are described in the supplementary material. All phase diagrams were measured at equal volumes of polar and non-polar phase ($\phi = 0.50$) and with the inclusion of NaCl at a mass fraction of salt in the polar phase of $w_{NaCl} = 0.001$ to screen ionic impurities stemming from reaction byproducts. The lamellar phase has been identified by its optical anisotropic lamellar domains observed with crossed polarizers. The analysis of the phase behavior is followed by a systematic small angle neutron scattering (SANS) and neutron spin echo (NSE) study of the polymer P(BO/EO)22 to reveal its mode of operation. The characteristic length scales and elastic properties of the membrane have been obtained with the neutron scattering techniques in the one-phase region of the phase diagram.

4.1 Phase Behavior

The first polymer tested is the diblock copolymer PBO5 - PEO5. Hence, the phase diagrams in figure 4.1 display the effect of the diblock at different weight fractions δ of copolymer within the amphiphile mixture ranging from zero to twenty percent. In the absence of polymer, the microemulsion exhibits typical non-ionic phase behavior as known from literature (compare e.g. [5]) with a bulky lamellar L_α - phase region in the middle of the one phase region (1) that is more stable at lower temperatures. The phase inversion temperature of the pure microemulsion is highlighted with a red dashed line in all figures to come to improve the visibility of possible temperature shifts induced by the polymer. Considering polymers like PEP5 - PEO5 [8], the majority of the polymers used here differ regarding the hydrophobic block as it is no pure polyalkylene, but a hydrophobic polyalkylene oxide. To our knowledge, the boosting capabilities of such polymers have not been studied before. If five weight percent of the surfactant are replaced with PBO5 - PEO5 three key aspects of the phase behavior change, while the system retains its phase inversion temperature and the non-ionic phase sequence. As to be expected, the amount of surfactant required to produce a one phase region decreases from $\gamma = (0.141 \pm 0.005)$ to $\gamma = (0.084 \pm 0.005)$, simultaneously, the dominance of the lamellar phase decreases. This is indicated by absence of deformation of the lower phase boundary and by a regression of the lamellar phase from $\gamma(L_\alpha) = (0.233 \pm 0.005)$ to $\gamma(L_\alpha) = (0.235 \pm 0.005)$. While this at first sight might not seem to be regression of the lamellar

phase in absolute terms of surfactant mass fraction, the distance of the lamellar phase to the phase boundaries of the one phase region increases from $\Delta\gamma(\delta = 0.00) = (0.092\pm0.005)$ to $\Delta\gamma(\delta = 0.05) = (0.151\pm0.005)$, resulting in a more extended one phase region. Upon increasing the polymer content to ten percent of the amphiphile mixture (note that δ is the fraction of the polymer in the membrane, not in the whole sample) the solubilization capacity grows even further to $\gamma = (0.058\pm0.005)$ without an observable shift in phase inversion temperature, while the shape of the lamellar phase changes from the previously bulky one, that resembles the shape of the one phase region, to a more elongated, almost needle-like shape, that extends to lower surfactant contents $\gamma(L_\alpha) = (0.165\pm0.005)$. As the gap between lamellar and one phase region is not significantly smaller with $\Delta\gamma(\delta = 0.10) = (0.107\pm0.005)$ it is safe to assume, that the lamellar phase is growing more dominant. This dominance is fully exerted if the polymer content is increased to twenty percent. Here hardly any microemulsion phase is present (lower part of Fig. 4.1). The isotropic one phase region is almost exclusively covered by a variety of liquid crystalline mesophases. The change of hydrophobicity of PBO-PEO (wrt. PEP-PEO) first extends the one-phase region, but leads to an extended lamellar phase at higher concentrations.

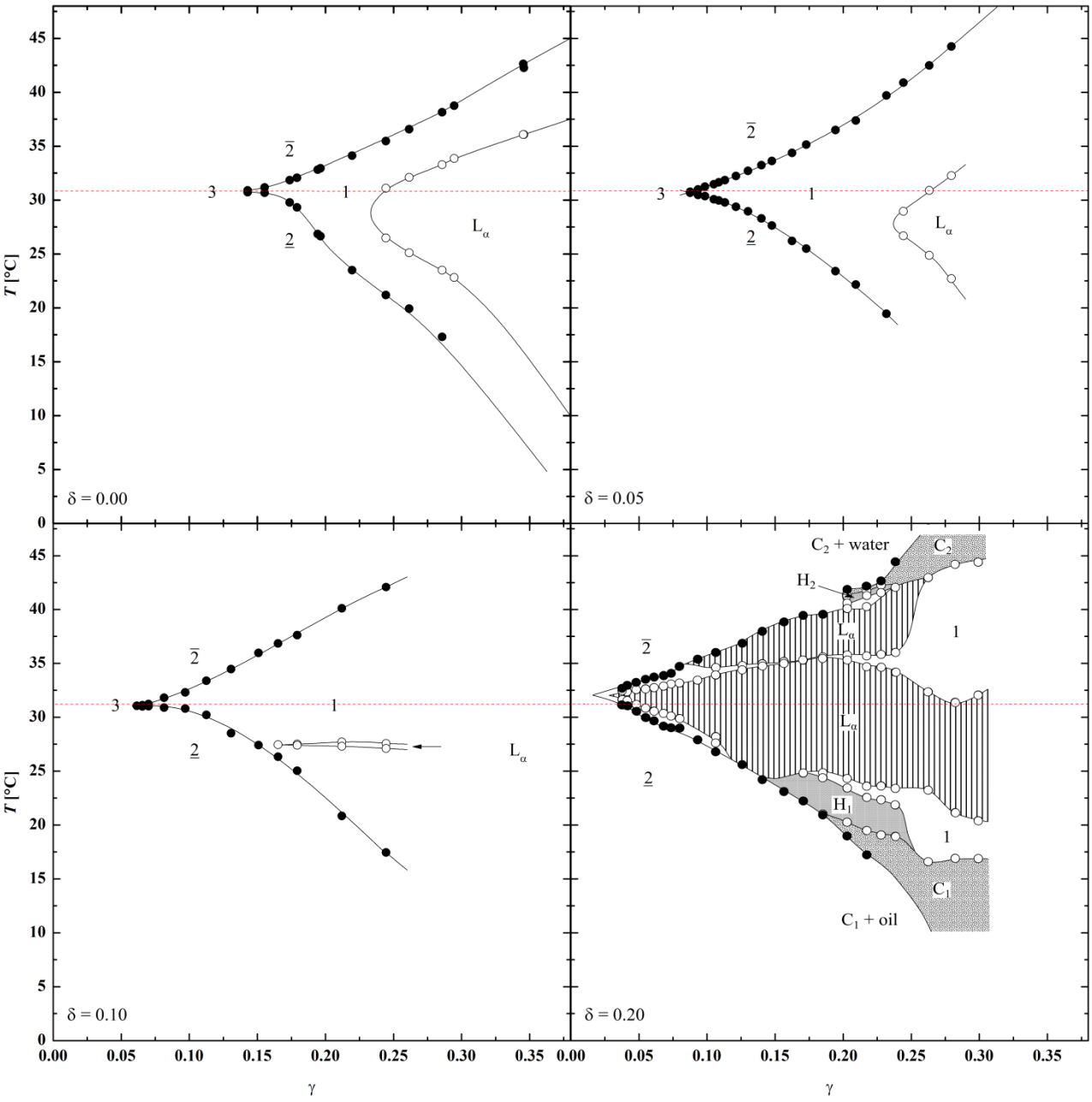

Figure 4.1: Phase diagrams as a function of temperature T and the overall mass fraction γ of the quaternary microemulsion of the system H_2O/NaCl - *n*-decane - $C_{10}E_4$/PBO5 - PEO5 with a symmetric oil to oil and water volume ratio $\phi = 0.50$ and a small quantity of salt in the polar phase ($w_{NaCl} = 0.001$) to screen electrostatic interactions due to impurities. The systems exhibit a non-ionic phase sequence and at high surfactant loads a dominant lamellar L_α - phase can be observed. The phase inversion temperature of the pure model system is highlighted by a red dashed line. The labels 1, $\underline{2}/\overline{2}$ and 3 denote the 1-phase/2-phase/3-phase region of the phase diagram. Hexagonal and cubic phases are denoted with an H and C respectively. We focus here only on the bicontinuous 1-phase region and the lamellar L_α-phase, for further details we refer to the literature[37].

It is to be noted, that most of the related two phase regions were too narrow to be resolved within the resolution limit of $\Delta T = 0.05$ °C. (This is a common occurrence when studying microemulsions in general and microemulsions including amphiphilic polymers in particular.

It originates in the fact that within e.g. the one phase region a gradual curvature change occurs as temperatures changes. So within a one phase region the structure changes continuously until the geometry of the membrane is broken and the structure changes into another one e.g. the instability of the lamellar phase compared to the bicontinuous structure (compare e.g. [4-6, 10]). Close to the slightly elevated phase inversion temperature, a vast lamellar L_α phase stretches almost till the total extend of the one phase region ($\Delta\gamma(\delta = 0.20) = (0.031 \pm 0.005)$). Symmetrically distributed around the phase inversion temperature are a hexagonal H_1 and an inverse hexagonal H_2 phase at mediocre surfactant content and low or high temperatures, respectively, and a micellar cubic C_1 and inverse micellar cubic C_2 phase at even higher surfactant content (for more details regarding the phase behavior see the supplementary material). Considering the shape and symmetry of the occurring phases, the behavior found here is typical for highly efficient microemulsions as known from literature and as to be expected for common polymers like PEP5 - PEO5. For comparison the technical diblock copolymer PEB4.8 - PEO4.8 can be found in the supplementary section.

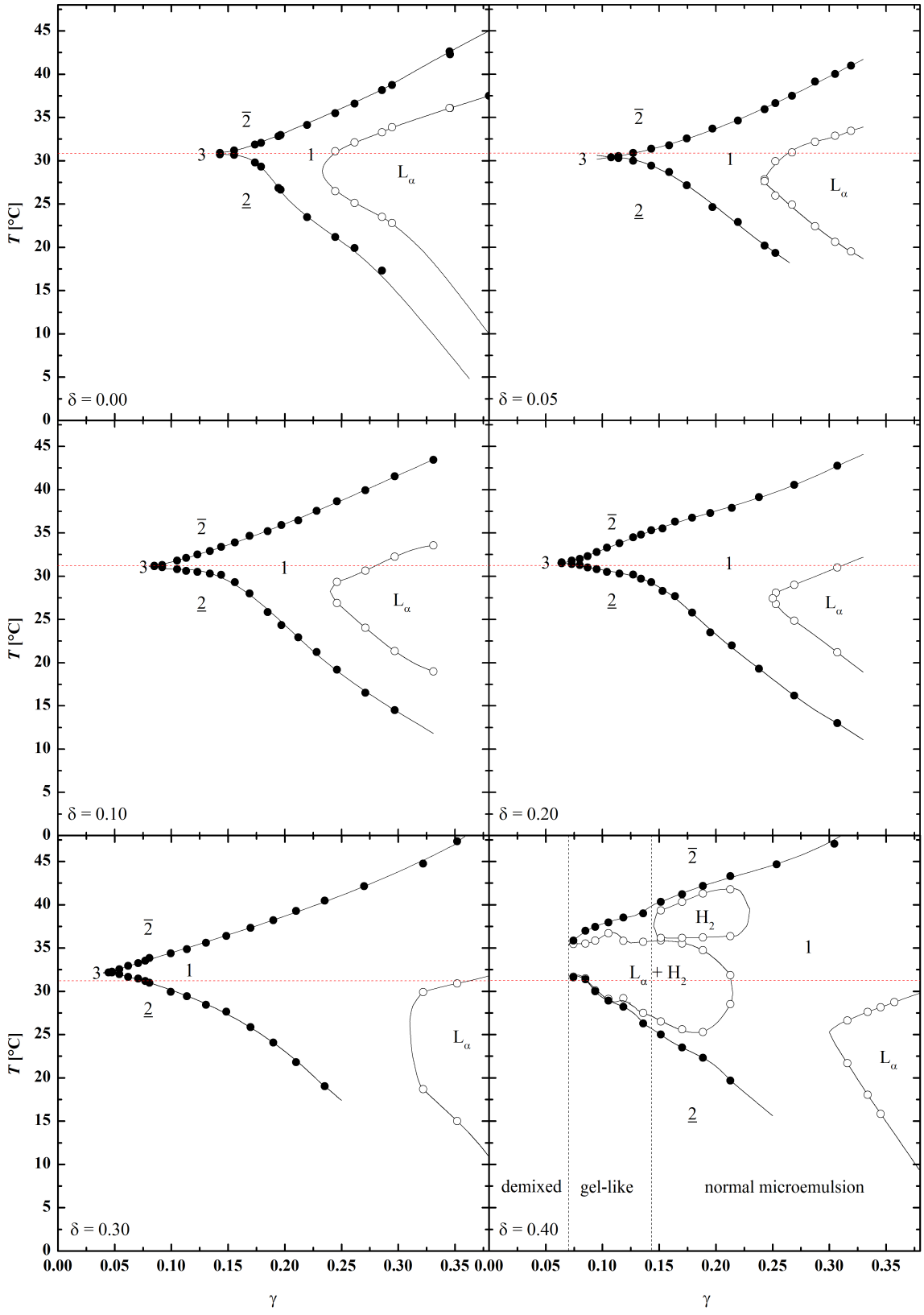

Figure 4.2: Phase diagrams of the system H_2O/NaCl - *n*-decane - $C_{10}E_4$/ P(BO/EO)22. Besides the nature of the polymer nothing was changed compared to figure 4.1. However, while the diblock copolymer promotes the formation of liquid crystalline mesophases at high polymer content, here their formation is suppressed significantly.

The gradient polymer P(BO/EO)22 was tested next. Here for polymer contents below thirty percent, the solubilization capacity increases, while the extension of the lamellar phase does not change much resulting in a wider one phase region. While for diblock copolymer concentrations above twenty percent no microemulsion was observable anymore, with P(BO/EO)22 even polymer contents up to forty percent are possible. Astonishingly, at thirty percent of polymer, the solubilization capacity of the microemulsion continues to increase and the lamellar phase decreases in extension even further above 31% of overall amphiphile mixture. Just at a polymer content of forty percent, a lamellar two phase state appears close to the closing point of the one phase region. Here, as depicted in figure 4.4 another phenomenon unknown so far occurs: for amphiphile contents below 14% the microemulsion turns into a gel-like state for the whole one phase region and does not form at all for amphiphile contents below seven percent. For the other triblock polymers tracing the change from pure diblock to gradient polymer we refer to the supplementary material.

4.2 Neutron scattering studies

Comparing the trends visible in figures 4.1 and 4.2 the most striking aspect is, that liquid crystalline phases are strongly suppressed for P(BO/EO)22, while increasing the solubilization capacity of the overall amphiphilic mixture dramatically. To further elucidate this matter systematic SANS and NSE studies were performed. While the other polymers with different intermediate block lengths were at hand, we did not see a need for detailed scattering experiment on them, because the differences to the diblock copolymer were too low (see also Fig. 4.1). SANS and NSE data are measured as a function of the absolute value q of the scattering vector **q**, which relates to real space distances d as $q=2\pi/d$.

Following the influence of polymer at a constant volume fraction of internal interface $\phi_{C+D} = 0.151$ at the maximum extend of the one phase region of the polymer free microemulsion and hence the phase inversion temperature the structure is expected to be bicontinuous [38]. As shown in figure 4.3 in the absence of polymer the scattering intensity starts at incoherent scattering at very high *q*-values turning into a slope of q^{-4}. At intermediate *q*-values this slope ends in a very pronounced peak that is accompanied by first order multiple scattering at twice the peak position. Going to even lower *q*-values the peak declines quickly leveling to a constant scattering intensity thereby yielding the typical scattering behavior of a bicontinuous structure. Despite the fact that the samples were only 0.1 mm thick multiple scattering could not be completely suppressed here, on the other hand the parameter

extraction from SANS takes place at the peak position and is not affected by multiple scattering processes with twice the q value. If the content of amphiphilic polymer is increased at constant ϕ_{C+D} the general shape of the scattering curves remains the same. However, with growing polymer content the sharpness and the height of the scattering peak increases indicating a more pronounced structure of higher order. Simultaneously the peak position shifts to lower *q*-values implying a growth in structure size.

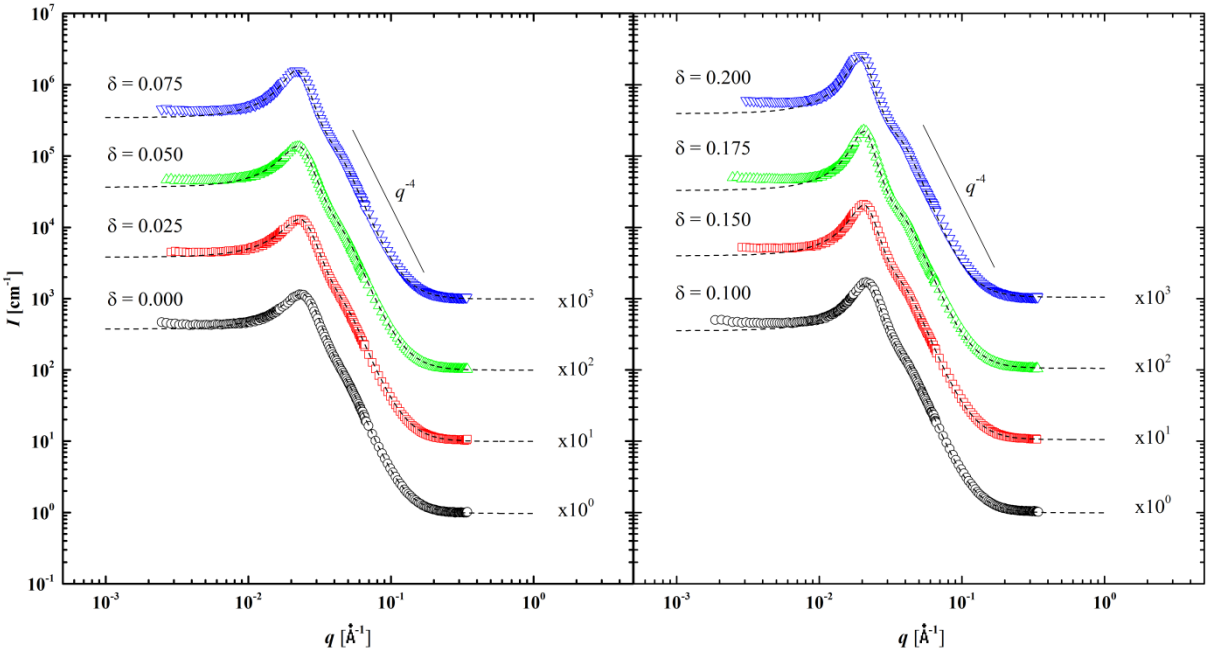

Figure 4.3: Overview of the absolute SANS-data *I*(*q*) of the microemulsion D_2O/NaCl - *n*-decane - $C_{10}E_4$/P(BO/EO)22 with a constant oil to oil and heavy water volume ratio $\phi = 0.50$ and a salt to salt and heavy water ratio $\varepsilon = 0.0009$. All sample were prepared such, that the overall surfactant volume ratio $\phi_{C+D} = 0.151$, which is close to the optimal point of the microemulsion without polymer, was kept constant. The polymer to polymer and surfactant ratio was varied such, that a range from 0-20% was crossed in 2.5% steps. Note that the sample of 12.5% was corrupted and is not shown here. Further data exists for higher polymer content. The data is described with a *Teubner-Strey* model for bicontinuous structures extended for short range fluctuations according to *Frank, Frielinghaus et al. (Ref. 39)*. The data is scaled as noted in the diagram for a better overview.

Based on the general observations the scattering behavior in figure 4.3 can be quantitatively described using the *Teubner-Strey* model [38] and by accounting for short range fluctuations as proposed by *Frank, Frielinghaus et al.* [39]:

$$I(q) = \left(\frac{8\pi c_2 \langle \eta^2 \rangle / \xi_{TS}}{a_2 + c_1 q^2 + c_2 q^4} + \frac{G \cdot erf^{12}(1.06 q R_G / \sqrt{6})}{1.5 q^4 {R_G}^4} \right) e^{-q^2 t^2} + I_{incoh.} \qquad (7)$$

with the correlation length ξ_{TS} being

$$\xi_{TS} = \left(\frac{1}{2}\left(\frac{a_2}{c_2}\right)^{1/2} + \frac{c_1}{4c_2}\right)^{-1/2} \tag{8}$$

and the characteristic domain size d_{TS} being

$$d_{TS} = 2\pi\left(\frac{1}{2}\left(\frac{a_2}{c_2}\right)^{1/2} - \frac{c_1}{4c_2}\right)^{-1/2} \tag{9}$$

with the parameters a_2, c_1 and c_2 stemming from a semi empiric series expansion and $\langle\eta^2\rangle = \phi_1\phi_2\Delta\rho^2$ describing the average fluctuations in scattering length density in a two phase system containing the phases 1 and 2. The short range fluctuations are described by their radius of gyration R_{G}, the amplitude G of the fractal *Beaucage* term and the interfacial roughness t. The quality of the structure in bulk contrast is closely related to the parameter c_1 and as long as it remains positive the well pronounced scattering peak of the bicontinuous structure occurs. To describe the quality of this structure the amphiphilicity factor f_{A} was introduced as

$$f_A = \frac{c_1}{\sqrt{4a_2c_2}} \tag{10}$$

ranging from -1 for perfectly structured crystals or lamellar phases to above +1 where critical phenomena occur. Considering the structural evolution occurring in both cases shown above ξ_{TS}, d_{TS} and f_{A} can be easily extracted from the scattering data and are given in figures 4.4 (for the data see tables S.1 in the supplementary material).

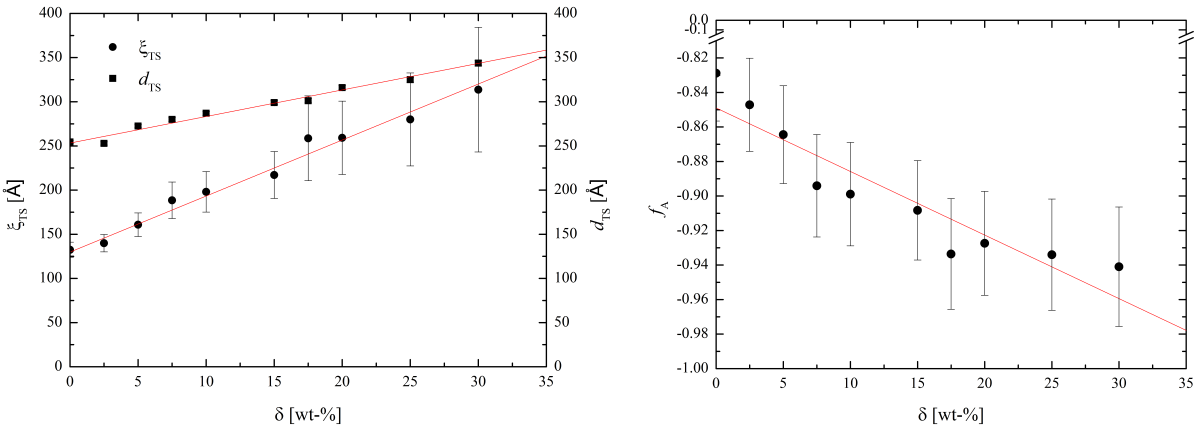

Figure 4.4: Comparison of the domain size d_{TS} and the correlation length ξ_{TS} (left) derived from the *Teubner-Strey* fits shown in Figure 4.3 as a function of polymer mass fraction δ. The corresponding amphiphilicity factor

is given on the right. The red lines correspond to linear regressions of the data as is intended as a guide for the eye.

In case of the microemulsion system at constant amphiphile volume fraction both the correlation length and the domain size increase linearly with growing polymer content. While one would expect the domain size to remain constant based on the assumedly constant amount of internal interface, the growth in domain size implies that the polymer is participating much less in the formation of internal interface itself but rather decorates the interface. This was also confirmed by normal as well as invariant *Porod* analysis [40] of the scattering data to extract the amount of total internal interface which can be rescaled with the polymer fraction to yield a constant *S*/*V* value for all polymer contents (compare supplementary figure S.4). In comparison to this growth in structure size the periodicity increases more strongly resulting in a better structurization of the sample that results in a crossover of both linear trends slightly above 35% of polymer present. The amphiphilicity factor approaches -1 in a similar fashion.

To further understand the effect of gradient polymer on the membrane and its suppression of the formation of lamellar phases one can extract the renormalized bending rigidity κ_{eff} and the renormalized *Gaussian* modulus $\bar{\kappa}_{\mathrm{eff}}$ from the scattering data as function of surface coverage $\sigma \cdot (R^2_{\mathrm{ee,w}} + R^2_{\mathrm{ee,o}})$ according to *Safran* and *Pieruschka* [41-44] based on:

$$\kappa_{SANS} = \frac{10\pi\sqrt{3}}{64}\frac{\xi_{TS}}{d_{TS}} - \frac{\alpha}{4\pi}\ln(1-\delta) \tag{11}$$

with corrections for the real surfactant content and based on *Morse*'s expression

$$\bar{\kappa}_{eff} = -\frac{\bar{\alpha}}{4\pi}\ln(\psi) \tag{12}$$

with ψ being the bare membrane fraction γ (1-δ) - 0.01 accounting for the real surfactant content minus the unimer solubility, and α=3, $\bar{\alpha}$ = -10/3. Using said equations and the plots of κ_{SANS} shown below calculated according to equation (11) the membrane parameters of the pure membrane can be calculated as $\kappa_0 = 0.44\ k_B T$ and $\bar{\kappa}_0 = -0.56\ k_B T$. These values are in good agreement with literature values e.g. by *Jakobs* and *Gompper* [15]. The change in bending rigidity as a function of surface coverage (i.e. the slope in Fig. 4.5, left) is with a value of 0.263 smaller than the same value for diblock polymers of 0.45 (from Ref. [17]). In the discussion the diblock polymer and the gradient polymer are compared in more detail.

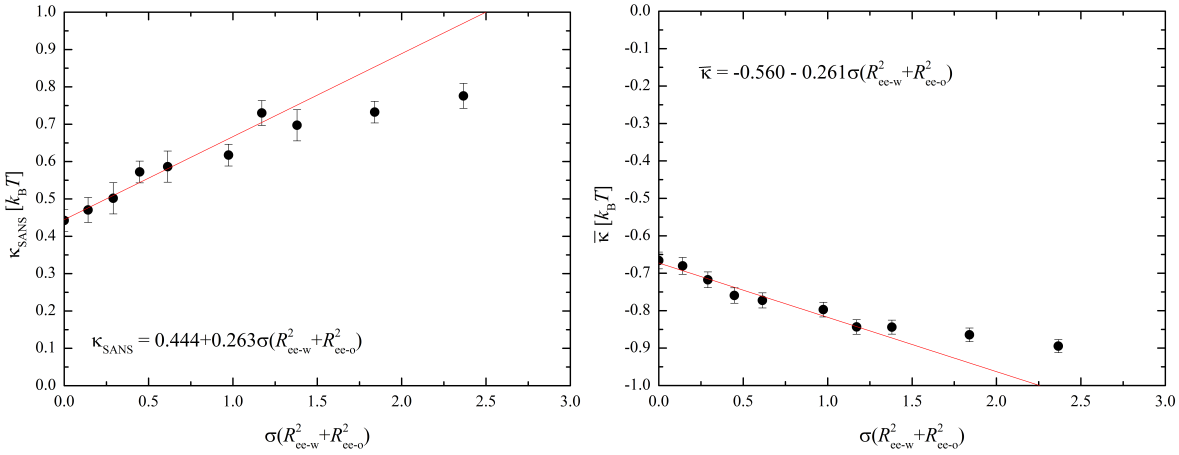

Figure 4.5: Left: The experimentally determined bending rigidity κ_{eff} (left) derived from the *Teubner-Strey* fits shown in Figure 4.3 as a function of the surface coverage $\sigma(R^2_{ee,w} + R^2_{ee,o})$. Right: The calculated saddle splay modulus $\bar{\kappa}_{eff}$ (left) derived from the *Teubner-Strey* fits shown in Figure 4.3 as a function of the surface coverage $\sigma(R^2_{ee,w} + R^2_{ee,o})$. The red lines correspond to linear regressions of the data. In both cases the black data was recorded for a constant amphiphile volume fraction of 0.151.

Following the trends depicted on the left of figure 4.3 the bending rigidity increases linearly with growing polymer content at constant amphiphile volume fraction. At $\sigma R^2_{ee} > 1.5$, deviations from the linear behavior indicate the polymer brush regime, where polymers along the membrane come into contact and interact repulsively. At the same time, the saddle splay modulus decreases linearly with growing surface coverage, until the brush regime is reached. Hence, while the membrane stiffens at high amphiphile content it does not do as strong as it would do in case of a normal diblock copolymer resulting in liquid crystaline phases and at the same time the formation of saddle points is even favorable at low amphiphile content in the systems with increased efficiency. This results in the suppression of liquid crystaline phases at low amphiphile content while at high content the formation of such phases is not enhanced compared to the polymer free system, until the brush regime is reached and gelling appears.

To confirm the findings based on the calculated membrane parameters NSE measurements were performed. The neutron spin echo (NSE) experiments have been conducted at the SNS-NSE instrument[45] at the spallation neutron source at the Oak Ridge National Laboratory (ORNL). NSE probes the characteristic time- and length-scales of thermal fluctuations, *i.e.* in the nanosecond and nanometer range. In the case of surfactant membrane dynamics, the intermediate scattering function $S(q,\tau)$ is the *Fourier* transform of the height correlation function of the membrane and allows to determine the bare bending rigidity κ_{NSE} of the membrane [46] as the only free parameter of the fitting function. At large scattering vectors q,

approximately $q>4q_0$ (i.e.>0.12 A^{-1}) the intermediate scattering function is not affected by the structural features of the microemulsion and reflects the height fluctuations of a small patch of the surfactant membrane. The often used final approximation of the expression derived by Zilman and Granek[46] for large bending rigidities is a simple stretched exponential decay of the normalized intermediate scattering function, $S(q,\tau)/S(q,0)=\exp(-(G\tau)^{\beta})$. For smaller values of the bending rigidity κ_{NSE} of the order of k_BT a numerical evaluation of the Fourier transformed height correlation function is needed, where κ_{NSE} is then the only fitting parameter. For a detailed description of the evaluation procedure we refer to Ref. [35].

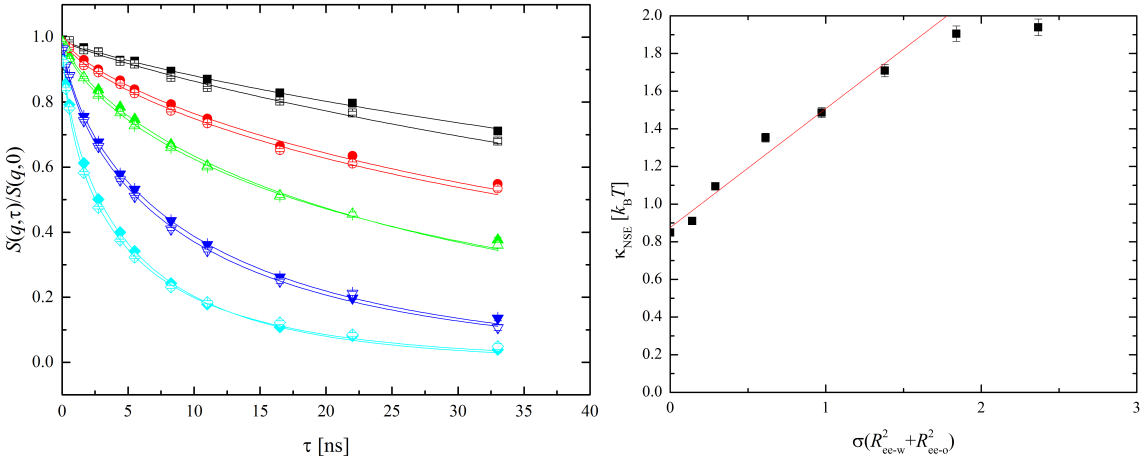

Figure 4.6: Intermediate scattering function of the samples with $\sigma\left(R_{ee,w}^2 + R_{ee,o}^2\right) = 0$ (full symbols) and $\sigma\left(R_{ee,w}^2 + R_{ee,o}^2\right) = 2.36$ (hollow symbols) for $q = 0.059$, 0.080. 0.098, 0.135 and 0.172 $Å^{-1}$ respectively (top to bottom), and the Bending rigidity κ_{NSE} as a function of surface coverage $\sigma\left(R_{ee,w}^2 + R_{ee,o}^2\right)$.

Figure 4.6 shows the intermediate scattering function for the lowest (zero) and highest polymer concentration and the resulting bending rigidity.. It has to be pointed out that the variation with surface coverage is systematic despite the small changes in sample composition and also in the relaxation rates, owing to the excellent stability of the instrument.

The bending rigidity κ_{NSE} increases linearly with polymer concentration until the brush regime is reached at $\sigma R_{ee}^2 \approx 1.5$. While neutron spin echo spectroscopy measures the membrane fluctuations, and therefore obtains a rather bare bending rigidity, the small angle scattering experiments give rise to an effective bending rigidity, which contains more contributions than only the original *Helfrich* bending rigidity [47, 48]. The bending rigidity from SANS is a mixture of the pure bending rigidity and the saddle splay modulus, renormalized due to the lengthscale where κ_{SANS} is measured. In the following discussion, we apply the corrections of κ_{SANS} as determined in Ref. [48], for details we refer to this reference.

5. Discussion and Summary

There are many details about the microemulsions with the different polymers added. All phase diagrams show increased efficiency when the amphiphilic polymers were added. But the tendency to form liquid crystalline phases was suppressed when the PPO block gained importance until the gradient polymer P(BO/EO)22 allowed for incredibly high polymer concentrations without formation of a lamellar phase. From the phase diagrams, the critical surfactant concentration was obtained that allowed to determine the sensitivity coefficient of the saddle splay modulus $\bar{\Xi}$ that displays the sensitivity of the saddle splay modulus upon the polymer addition. All coefficients of the diblock copolymer and gradient polymer are summarized in table 5.1, while the survey plot was already shown in figure 2.1. For the gradient polymer the coefficient $\bar{\Xi}$ was smaller by a factor of 0.64 than for the diblock copolymer. This agrees rather well with the predictions from our calculations where we found a weaker dependence by a factor of 0.75. The path to the theoretical description of the influence of the anchoring point is shown in the supplementary material X.6. The value Ξ is calculated as a function of anchoring point (solid lines in Fig. 2.1). The comparison with experiment is summarized in table 5.1.

Apart from that, the analysis of the bending rigidity is supported by neutron scattering experiments. The values obtained by neutron spin echo (NSE) spectroscopy relate to dynamic properties, where we found a nearly unchanged coefficient for the gradient polymer compared to the diblock copolymer. The theoretical estimation would only predict a by 0.70 smaller coefficient for the gradient polymer. In parallel we discuss the corrections of the coefficients to Ξ_{SANS}. The bare coefficient $\Xi_{SANS\text{-}bare} = (\Xi_{SANS} - 0.85\bar{\Xi})/0.15$ (corrections introduced in references [47] and [48]) of the gradient polymer differs not much from the other original coefficients Ξ_{SANS} and $\bar{\Xi}$, but is a considerably (0.4 times) lower than the corresponding diblock copolymer value (and than Ξ_{NSE}).

For the gradient P(BO/EO)22 polymer we find a dynamically nearly unchanged value Ξ with respect to the diblock copolymer. This indicates the possibly that the polymer is dynamically locked in smaller compartments along the chain, because the monomer sequences are either fully hydrophilic or hydrophobic. Then, the two locked polymer blocks dynamically act like an ideal diblock copolymer, where the anchoring point is not ideally symmetric but dynamically rather stable. However, structurally, the different rather stable anchoring points along the membrane in concert with the neighboring slightly confining membranes give the

central membrane additional excitations with respect to the centre due to the random different sizes of the two blocks. Structurally, the membrane appears to be stronger fluctuating, while dynamically this is not the case at all. However, the averaged effect of $\Xi \approx 0.77$ seems to meet our theoretical expectations. We would like to stress, that we do not expect such a splitting for the triblock polymers with intermediately polar middle blocks, but the deviations from the diblock value would be small anyhow. Apart from that, the coefficient of the saddle splay modulus $\bar{\Xi}$ seems to show no splitting.

Table 5.1: Comparison of the sensitivity coefficients of the saddle-splay modulus, and the bending rigidity (determined from NSE and SANS, and a corrected value). The last column displays the theoretical ratio of the coefficients between the gradient and diblock copolymer. Diblock copolymer values are from [17]. All errors are 10% or less.

Coefficient	Diblock Copolymer	Gradient Polymer	Experimental and Predicted Ratio Gradient / Diblock
$\bar{\Xi}$	0.41	0.261	0.64 | 0.75
Ξ_{NSE}	0.56	0.631	1.13 | 0.70
Ξ_{SANS}	0.45	0.263	0.58 | ?.??
$\Xi_{SANS\text{-}bare}$	0.68	0.274	0.40 | 0.70

Looking back on the suppression of the liquid crystalline phases with increasingly soft crossover from hydrophilic to hydrophobic part of the polymer, or reduced εN^2 parameter, we have to discuss the two parameters $2\kappa + \bar{\kappa}$ and $-\bar{\kappa}$ [49]. The first one would support overall less curved membranes. It is growing anyhow in all our cases, be it a little faster or slower. If the latter parameter is small, it would favor minimal surfaces, i.e. the bicontinuous phase, contrarily to the lamellar phase when $-\bar{\kappa}$ becomes large. We observed and predicted a smaller growth of $-\bar{\kappa}$ with reduced anchoring strength εN^2, which directly leaves the lamellar phase further away at higher surfactant concentrations. The faster growth of the dynamic κ from NSE experiments supports the observed higher efficiency for gradient diblock copolymers, while the static picture would not explain the observations. Thus the dynamic appearance of thermodynamic systems must be analyzed to explain the macroscopic behavior. The obvious effect of the blockiness of the tapering on dynamic properties was also confirmed in computer simulations on translocating polymers through lipid bilayers [50].

We can summarize that the class of gradient polymers cause a stiffening of the amphiphilic film similar to diblock polymers, while simultaneously the saddle splay modulus behaves differently from the diblock polymers with a much smaller change upon gradient polymer addition. As a result, the formation of liquid crystalline mesophases is suppressed while bicontinuous structures are geometrically favoured. Hence gradient amphiphilic polymers not only increase the efficiency of surfactants but simultaneously suppress the formation of liquid crystalline phases thereby greatly increasing their application potential.

6. Acknowledgement

The authors wish to thank Thomas Sottmann for helpful discussions and initiating this work.

This research at ORNL's Spallation Neutron Source was sponsored by the Scientific User Facilities Division, Office of Basic Energy Sciences, U.S. Department of Energy.

This work is based upon experiments performed at the KWS-1 instrument operated by JCNS at the Heinz Maier-Leibnitz Zentrum (MLZ), Garching, Germany.

The authors gratefully acknowledge the financial support provided by JCNS to perform the neutron scattering measurements at the Heinz Maier-Leibnitz Zentrum (MLZ), Garching, Germany.

7. Statement on Disclosure of potential conflicts of interest

All authors declare that they have no conflict of interests.

7. Literature

1. K. Shinoda and S. Friberg, *Adv. Colloid Interface Sci.*, 1975, **4**, 281-300.
2. P. A. Winsor, *Solvent Properties of Amphiphilic Compounds*, Buttersworth, London, 1954.
3. H. Arai and K. Shinoda, *J. Colloid Interface Sci.*, 1967, **25**, 396-&.
4. M. Kahlweit and R. Strey, *Angew. Chem.-Int. Edit. Engl.*, 1985, **24**, 654-668.
5. M. Kahlweit, R. Strey, D. Haase, H. Kunieda, T. Schmeling, B. Faulhaber, M. Borkovec, H. F. Eicke, G. Busse, F. Eggers, T. Funck, H. Richmann, L. Magid, O. Soderman, P. Stilbs, J. Winkler, A. Dittrich and W. Jahn, *J. Colloid Interface Sci.*, 1987, **118**, 436-453.
6. M. Kahlweit, R. Strey and G. Busse, *Journal of Physical Chemistry*, 1990, **94**, 3881-3894.
7. M. Kahlweit, R. Strey and G. Busse, *Physical Review E*, 1993, **47**, 4197-4209.
8. B. Jakobs, T. Sottmann, R. Strey, J. Allgaier, L. Willner and D. Richter, *Langmuir*, 1999, **15**, 6707-6711.
9. H. Kunieda and K. Shinoda, *J Disper Sci Technol*, 1982, **3**, 233-244.
10. C. Stubenrauch, C. Frank, R. Strey, D. Burgemeister and C. Schmidt, *Langmuir*, 2002, **18**, 5027-5030.
11. C. Frank, T. Sottmann, C. Stubenrauch, J. Allgaier and R. Strey, *Langmuir*, 2005, **21**, 9058-9067.
12. C. Frank, R. Strey, C. Schmidt and C. Stubenrauch, *J. Colloid Interface Sci.*, 2007, **312**, 76-86.
13. B. Jakobs, T. Sottmann and R. Strey, *Tenside Surfactants Deterg.*, 2000, **37**, 357-364.
14. H. Endo, J. Allgaier, G. Gompper, B. Jakobs, M. Monkenbusch, D. Richter, T. Sottmann and R. Strey, *Physical Review Letters*, 2000, **85**, 102-105.
15. G. Gompper, H. Endo, M. Mihailescu, J. Allgaier, M. Monkenbusch, D. Richter, B. Jakobs, T. Sottmann and R. Strey, *Europhysics Letters*, 2001, **56**, 683-689.
16. C. Frank, H. Frielinghaus, J. Allgaier and D. Richter, *Langmuir*, 2008, **24**, 6036-6043.
17. M. Brodeck, S. Maccarrone, D. Saha, L. Willner, J. Allgaier, G. Mangiapia, H. Frielinghaus, O. Holderer, A. Faraone and D. Richter, *Colloid and Polymer Science*, 2015, **293**, 1253-1265.
18. N. Nuraje, H. Bai and K. Su, *Progress in Polymer Science*, 2013, **38**, 302-343.
19. L. Ionov, B. Zdyrko, A. Sidorenko, S. Minko, V. Klep, I. Luzinov and M. Stamm, *Macromolecular Rapid Communications*, 2004, **25**, 360-365.
20. S. J. Lord, S. S. Sheiko, I. LaRue, H. I. Lee and K. Matyjaszewski, *Macromolecules*, 2004, **37**, 4235-4240.
21. G. Moad, E. Rizzardo and S. H. Thang, *Australian Journal of Chemistry*, 2005, **58**, 379-410.
22. M. Daoud and J. P. Cotton, *Journal De Physique*, 1982, **43**, 531-538.
23. L. Arleth, B. Svensson, K. Mortensen, J. S. Pedersen and U. Olsson, *Langmuir*, 2007, **23**, 2117-2125.
24. A. Kabalnov, B. Lindman, U. Olsson, L. Piculell, K. Thuresson and H. Wennerstrom, *Colloid and Polymer Science*, 1996, **274**, 297-308.
25. B. Lindman, P. Alexandridis, U. Olsson, L. Piculell and K. Thuresson, *Abstracts of Papers of the American Chemical Society*, 1996, **211**, 194-COLL.
26. R. Roy, J. K. Park, W.-S. Young, S. E. Mastroianni, M. v. S. Tureau and T. H. Epps, *Macromolecules*, 2011, **44**, 3910-3915.
27. N. Singh, M. S. Tureau and I. I. I. T. H. Epps, *Soft Matter*, 2009, **5**, 4757-4762.

28. K. Knoll and N. Nießner, *Macromolecular Symposia*, 1998, **132**, 231-243.
29. W. Zhang, J. Allgaier, R. Zorn and S. Willbold, *Macromolecules*, 2013, **46**, 3931-3938.
30. M. Breidenich, R. R. Netz and R. Lipowsky, *Europhysics Letters*, 2000, **49**, 431-437.
31. C. Hiergeist and R. Lipowsky, *Journal De Physique Ii*, 1996, **6**, 1465-1481.
32. R. Lipowsky, *Europhysics Letters*, 1995, **30**, 197-202.
33. R. Lipowsky, *Colloids and Surfaces a-Physicochemical and Engineering Aspects*, 1997, **128**, 255-264.
34. A. Hanke, E. Eisenriegler and S. Dietrich, *Physical Review E*, 1999, **59**, 6853-6878.
35. M. Mihailescu, M. Monkenbusch, H. Endo, J. Allgaier, G. Gompper, J. Stellbrink, D. Richter, B. Jakobs, T. Sottmann and B. Farago, *The Journal of Chemical Physics*, 2001, **115**, 9563-9577.
36. J. Allgaier, S. Willbold and T. H. Chang, *Macromolecules*, 2007, **40**, 518-525.
37. M. S. Leaver, U. Olsson, H. Wennerstrom, R. Strey and U. Wurz, *Journal of the Chemical Society, Faraday Transactions*, 1995, **91**, 4269-4274.
38. M. Teubner and R. Strey, *Journal of Chemical Physics*, 1987, **87**, 3195-3200.
39. C. Frank, H. Frielinghaus, J. Allgaier and H. Prast, *Langmuir*, 2007, **23**, 6526-6535.
40. O. Kratky and G. Porod, *Journal of Colloid Science*, 1949, **4**, 35-70.
41. P. Pieruschka and S. A. Safran, *Europhysics Letters*, 1993, **22**, 625-630.
42. P. Pieruschka and S. A. Safran, *Europhysics Letters*, 1995, **31**, 207-212.
43. P. Pieruschka and S. A. Safran, *Journal of Physics-Condensed Matter*, 1994, **6**, A357-A362.
44. P. Pieruschka, S. A. Safran and S. T. Marcelja, *Physical Review E*, 1995, **52**, 1245-1247.
45. M. Ohl, M. Monkenbusch, N. Arend, T. Kozielewski, G. Vehres, C. Tiemann, M. Butzek, H. Soltner, U. Giesen, R. Achten, H. Stelzer, B. Lindenau, A. Budwig, H. Kleines, M. Drochner, P. Kaemmerling, M. Wagener, R. Möller, E. B. Iverson, M. Sharp and D. Richter, *Nuclear Instruments and Methods in Physics Research Section A: Accelerators, Spectrometers, Detectors and Associated Equipment*, 2012, **696**, 85-99.
46. A. G. Zilman and R. Granek, *Physical Review Letters*, 1996, **77**, 4788-4791.
47. M. Peltomaeki, G. Gompper and D. M. Kroll, *Journal of Chemical Physics*, 2012, **136**.
48. O. Holderer, H. Frielinghaus, M. Monkenbusch, M. Klostermann, T. Sottmann and D. Richter, *Soft Matter*, 2013, **9**, 2308-2313.
49. G. Gompper and U. Schwarz, in *Morphology of Condensed Matter: Physics of Geometry of Spatially Complex Systems*, eds. K. Mecke and D. Stoyan, Springer Verlag, Heidelberg, Berlin and New York, 2002, pp. 107-151.
50. M. Werner and J.-U. Sommer, *Biomacromolecules*, 2015, **16**, 125-135.